

# Cooperative Motion of Active Brownian Spheres in Three-Dimensional Dense Suspensions

Adam Wysocki,<sup>1,\*</sup> Roland G. Winkler,<sup>1,†</sup> and Gerhard Gompper<sup>1,‡</sup>

<sup>1</sup>*Theoretical Soft Matter and Biophysics, Institute for Advanced Simulation and Institute of Complex Systems, Forschungszentrum Jülich, 52425 Jülich, Germany*

(Dated: July 22, 2022)

The structural and dynamical properties of suspensions of self-propelled Brownian particles of spherical shape are investigated in three spatial dimensions. For sufficiently large density and self-propulsion, the system is found to phase separate into a dilute and a dense phase. The packing fraction of dense phase may approach random close packing at high activity, but nevertheless it remains a fluid. Although polar order is absent, long-lived cooperative motion with nearly scale-free correlations is detected for systems with a density close to or above the glass transition density in passive systems.

PACS numbers: 82.70.Dd, 64.75.Xc, 47.63.Gd, 87.18.Hf

Assemblies of intrinsically active objects, sometimes called *living fluids*, represent an exceptional class of non-equilibrium systems. Examples range from the macroscopic scale of human crowds to the microscopic scale of cells and motile microorganisms such as bacteria [1, 2]. A generic phenomenon of dense living fluids is the emergence of self-organized large-scale dynamical patterns like vortices, swarms, networks or self-sustained turbulence [3–5]. This intriguing dynamical behavior is a consequence of the complex interplay of self-propulsion, internal or external noise, and many-body interactions.

The understanding of the collective behavior requires the characterization of the underlying physical interaction mechanisms. Experiments and simulations indicate that alignment induced by particle interactions, like inelastic collisions between elongated objects [5–7] or hydrodynamic interactions [8], lead to clustering and collective motion. Studies of rodlike self-propelled particles in two dimensions (2D) revealed mobile clusters and a variety of other dynamical phases [5–7]. In contrast, 2D systems of disc-like particles exhibit nearly immobile clusters [9–11] with an internal crystalline order [12].

Far less attention has been paid to three-dimensional (3D) suspensions of spherical (colloid-like) active particles. In such systems, the question naturally arises, whether a collective behavior emerges despite the particles lack any aligning interactions. In this letter, we present simulation results of the emergent structure and dynamics of motile spherical particles in 3D—as a generic model of non-aligning self-driven particles. We find that an isotropic system phase separates into a dilute, gas-like phase, and a dense, fluid-like phase at sufficiently large activity. In the dense phase, the particles exhibit collective motion even at densities very close to random close packing (RCP). Although a global polar order is absent in the system, long-lived cooperative motion with nearly scale-free correlations emerge.

We model an active particle as a smooth hard sphere (HS) which is propelled with constant velocity  $V_0$  along

its orientation vector  $\mathbf{e}$  [9, 11–13] in 3D. The translational motion is governed by  $\dot{\mathbf{r}} = V_0\mathbf{e} + \mathbf{F}_{HS}/\gamma_t + \eta$ , where  $\mathbf{F}_{HS}$  is the force due to HS interaction [14] and  $\eta$  is a random velocity with  $\langle \eta \rangle = 0$  and  $\langle \eta_i(t)\eta_j(t') \rangle = 2D_t\delta_{ij}\delta(t-t')$ . The orientation  $\mathbf{e}$  performs a random walk according to  $\dot{\mathbf{e}} = \xi \times \mathbf{e}$ , with  $\langle \xi \rangle = 0$  and  $\langle \xi_i(t)\xi_j(t') \rangle = 2D_r\delta_{ij}\delta(t-t')$ . The translational and rotational diffusion coefficients,  $D_t$  and  $D_r$ , of a HS of diameter  $\sigma$  are  $D_t = k_B T/\gamma_t = D_r\sigma^2/3$ . The importance of noise is measured by the Péclet number  $Pe = V_0/(\sigma D_r)$ . We study systems with  $Pe$  in a broad range of  $9 \leq Pe \leq 272$ . Up to  $N = 1.5 \times 10^5$  particles are simulated in a cubic box of length  $L$ . The density is measured in terms of the packing fraction  $\phi = \frac{4}{3}\pi(\frac{\sigma}{2})^3 \frac{N}{L^3}$ . A natural time scale is  $\tau_r = 1/(2D_r)$ . Our model mimics the main aspects of various real systems, such as thermo- or diffusio-phoretic spherical microswimmers [10, 11, 15–17] (with  $Pe \approx 7 - 200$ ), and persistently swimming spherical colonies of the green algae *Volvox* [18] (with  $Pe \approx 10^8$ ).

We first focus on a system with the large Péclet number  $Pe = 272$ . This system shows a remarkable phase behavior as function of the global packing fraction  $\phi$ . Figure 1(a) shows the probability distribution  $P_\phi$  of the local packing fraction  $\phi_{local}$  as a function of  $\phi$ , where  $\phi_{local}$  is obtained by Voronoi construction [19]. For  $\phi \lesssim \phi_c \approx 0.3375$ , the system is essentially homogeneous and  $P_\phi$  is unimodal. While approaching a critical packing fraction  $\phi_c$  with increasing  $\phi$ ,  $P_\phi$  broadens (by formation of transient clusters) and becomes bimodal above  $\phi_c$ , i.e., the system separates into a low-density gas phase and a high density fluid phase. Remarkably, the packing fraction in the fluid phase  $\phi_f \approx 0.62$  is very high, in particular, it is deep within the glassy region ( $\phi_G \approx 0.58 \leq \phi \leq \phi_{RCP} \approx 0.64$ ) of passive hard spheres [20, 21]; nevertheless, particles remain mobile and no long-range crystalline order is detected.

The morphology of the fluid phase ( $\phi_{local} > 0.52$ ) can be characterized by Minkowski functionals—the surface area  $A$ , the integrated mean curvature  $C$ , and the Eu-

ler characteristic  $\chi$  (for details see Ref. [22]). The average values of all functionals, as well as their fluctuations, rise dramatically with increasing  $\phi \rightarrow \phi_c$  due to enhanced formation of transient spherical ( $\chi > 0$ ) clusters, see Fig. 1(b-d). At  $\phi_c$ , the clusters start to form a percolating network and consequently  $\chi < 0$ ; the clustering transition appears to be continuous, i.e., the lifetime and the size of clusters diverge at  $\phi_c$ . With increasing  $\phi > \phi_c$ , the fluid phase forms first a nearly bicontinuous structure ( $\chi < 0$  and  $C < 0$ ), whose surface is reminiscent of the Schwarz P surface, and finally at high  $\phi$ , gas-phase droplets float in a dense matrix ( $\chi > 0$  and  $C < 0$ ). In contrast to an equilibrium system (away from the critical point) the morphology of the gas (or fluid) phase is highly dynamic as is reflected by the large fluctuations of  $\chi$ , i.e., the structures continuously merge and break.

The structure formation of motile hard sphere particles in 3D displays an essential difference compared to 2D: clusters in 2D are crystalline [12] at sufficiently high  $Pe$ , while clusters in 3D are fluid. Note that rapidly compressed hard spheres form a glass phase [23], which is absent in 2D for monodisperse discs. This has important consequences. In both cases, particles at the rim of the cluster point inward and hence exert pressure on the interior. However, in the 2D case, the interior cannot easily react to an inhomogeneous pressure distribution because of its finite elastic moduli. This is different for a fluid interior in 3D; a inhomogeneous pressure generates internal currents and a continuous deformation of the structure [24].

A dense environment, whether it is a cluster or a homogenous suspension, is a prerequisite for collective motion in active fluids. Indeed, the phase-separated systems reveal an intriguing dynamics within the fluid phase (cf. Fig. 2). Large-scale coherent displacement patterns emerge, with amplitudes and directions strongly varying spatially. In addition, transient swirl-like structures appear frequently. Figure 2(a) shows a swirl spanning the whole cluster while Fig. 2(b) provides an example of a large mobile region (red/orange) moving from top to bottom between the gas-phase regions of the system [24]. At first glance, this is surprising considering the fact that  $\phi_f \approx 0.62 > \phi_G \approx 0.58$ .

The particle dynamics reveals features of a self-sustained instability, i.e., it is heterogeneous in space and time. To characterize the correlated dynamics, we adopt the spatio-temporal correlation function [25]

$$C_d(r, \Delta t) = \frac{\left\langle \sum_{i,j \neq i} \mathbf{d}_i \cdot \mathbf{d}_j \delta(r - |\mathbf{r}_i - \mathbf{r}_j|) \right\rangle_t}{c_0 \left\langle \sum_{i,j \neq i} \delta(r - |\mathbf{r}_i - \mathbf{r}_j|) \right\rangle_t}, \quad (1)$$

where  $\mathbf{d}_i(t, \Delta t) = \mathbf{r}_i(t + \Delta t) - \mathbf{r}_i(t)$  is the displacement of particle  $i$  over a lag time  $\Delta t$  and  $c_0 = \langle \sum_i \mathbf{d}_i^2 / N \rangle_t$  is a normalization factor. Due to the finite system size

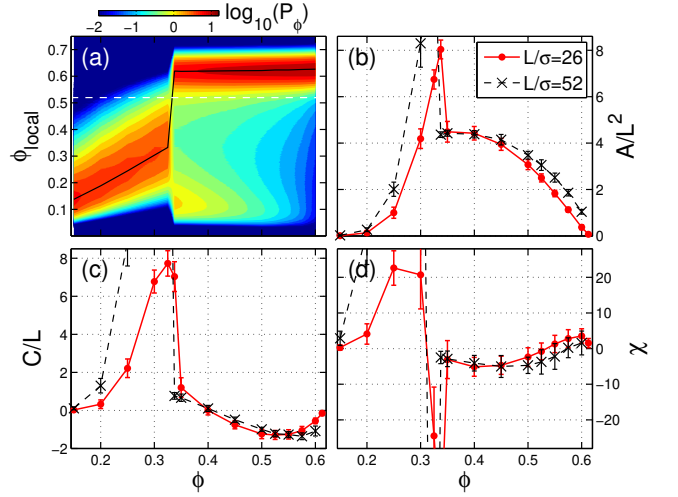


FIG. 1: (color online) (a) Probability distribution  $P_\phi$  of the local packing fraction  $\phi_{local}$  as a function of the global packing fraction  $\phi$  for  $Pe = 272$  and  $L/\sigma = 52$ . The most probable  $\phi_{local}$  is indicated by a solid black line,  $\phi_f \approx 0.62$  is deep within the glassy region for  $\phi > \phi_c$ . (b-c) Morphological analysis of the fluid phase ( $\phi_{local} > 0.52$  is indicated by a dashed line in (a)). Minkowski functionals, namely, (b) the interface area  $A$ , (c) the integrated mean curvature  $C$ , and (d) the Euler characteristic  $\chi$  versus  $\phi$  are shown.

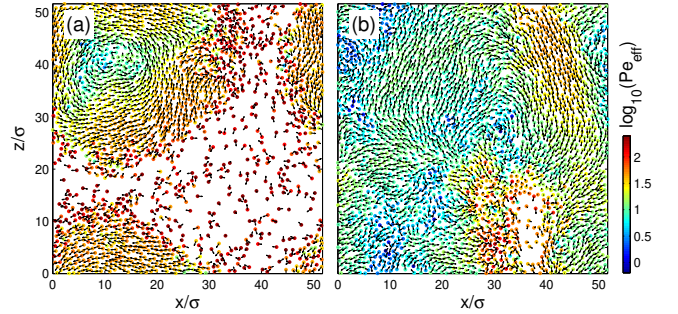


FIG. 2: (color online) Collective motion in the steady state at  $Pe = 272$ , see movies in [24]. Snapshots (slices of thickness  $\sigma$ ) of a system (a) just above the clustering transition ( $\phi = 0.3375$ ) and (b) at a high concentration ( $\phi = 0.6$ ). Arrows indicate the direction of the displacements  $\mathbf{d}(t, \Delta t) = \mathbf{r}(t + \Delta t) - \mathbf{r}(t)$  over a lag time  $\Delta t \approx 0.4\tau_r$ , while the magnitude  $d = |\mathbf{d}|$  is color-coded and is expressed as an effective Péclet number,  $Pe_{eff} = d/(\Delta t \sigma D_r)$ .

we measure  $\mathbf{d}$  in the center-of-mass reference frame. In the asymptotic limit  $\Delta t \rightarrow 0$ ,  $C_d(r, \Delta t)$  is proportional to equal-time spatial velocity correlation function. Moreover, we introduce the correlation length  $\xi_d(\Delta t)$  by the condition  $C_d(\xi_d, \Delta t) = 0$ , and a global measure of cooperative motion as

$$\chi_d(\Delta t) = \int_{\sigma}^{L/2} C_d(r, \Delta t) dr. \quad (2)$$

In the following, we focus exemplarily on a dense sys-

tem with  $\phi = 0.6$ , where on average one or two gas-phase droplets float within the fluid phase with  $\phi_f \approx 0.626$  (see Fig. 2(b)), although our conclusions are valid for most  $\phi > \phi_c$ . Figure 3(a) shows the correlation functions  $C_d$  for various system sizes at the time  $\tau$  of maximal cooperativity. The latter follows from  $\chi_d(\Delta t)$ , which exhibits a maximum at  $\Delta t = \tau$ , as indicated by symbols in Fig. 3(b). The correlations extend over a remarkably large part of the system; only for  $r \gtrsim 0.1L^{0.93}$ ,  $C_d$  decays exponentially and becomes finally negative. This corresponds to a backflow of particles, which can be attributed to the incompressibility of the fluid phase. The correlation length,  $\xi_d(\tau)$ , increases (nearly) linearly with system size  $L$  or, more precisely,  $\xi_d \sim L^{0.93}$ , cf. Fig. 3(c). This can be understood as an indication for scale invariance of  $C_d$  in the thermodynamic limit (long-range correlations), i.e.,  $C_d \sim r^{-\gamma}$  for  $L \rightarrow \infty$  [26, 27]. A fit to our data yields  $\gamma \approx 0.15$  and hence implies that correlations decay extremely slowly. Note that an accurate estimate of a small  $\gamma$  is difficult and requires huge system sizes. Our data scale reasonably well over the considered range; however, a cut-off length might exist on larger length scales. Similar behavior has also been observed for other active fluids such as starling flocks [26] and recently in motile bacteria colonies [27]; however, both systems exhibit notable polar alignment mechanisms.

The cooperative motion is not instantaneously present, it rather builds up with time. As indicated in Fig. 3(b),  $\chi_d(\Delta t)$  reaches a maximum at  $\tau$  and decays again. The bell-like shape of  $\chi_d(\Delta t)$  is characteristic for the dynamics in dense fluids [25]. At short times, particles move independently in their own cage (low correlation), but gradually particles feel the motion of their neighbours and the displacements become correlated over an increasing length scale. Interestingly,  $\tau$  depends on the system size and we observe a strong non-linear increase  $\tau \sim \exp(L/\xi)$  with  $\xi = 19\sigma$ , see Fig. 3(d). Hence, long-living, coherently moving domains are predicted for large systems.

The relation,  $\tau \sim \exp(\xi_d^{1.08})$ , between the build-up time  $\tau$  and the correlation length of the displacements  $\xi_d(\tau)$  indicates a connection to the glass transition. Recently, it has been suggested that the glass-transition is a critical-like phenomenon with an anomalously strong critical slowing down and a similar relation between the time and the length scale was predicted [28]. We speculate that the divergence of  $\tau$  and  $\xi_d$  with  $L$  in our case is associated with the fact that the packing fraction within clusters is above  $\phi_G$  and that an active perturbation of a system with  $\phi > \phi_G$  leads to a critical-like response.

We find only a weak relation between the cooperative motion and inter-particle correlations of the propulsion directions  $\mathbf{e}$ . The latter can be characterized by the function  $C_e(r)$ , where the vector  $\mathbf{d}$  is replaced by  $\mathbf{e}$  in Eq. (1). Although,  $C_e$  signals a long-range correlation, similar to  $C_d$ , with  $\xi_e \approx \xi_d$  (see Fig. 3(c)), the orientation correla-

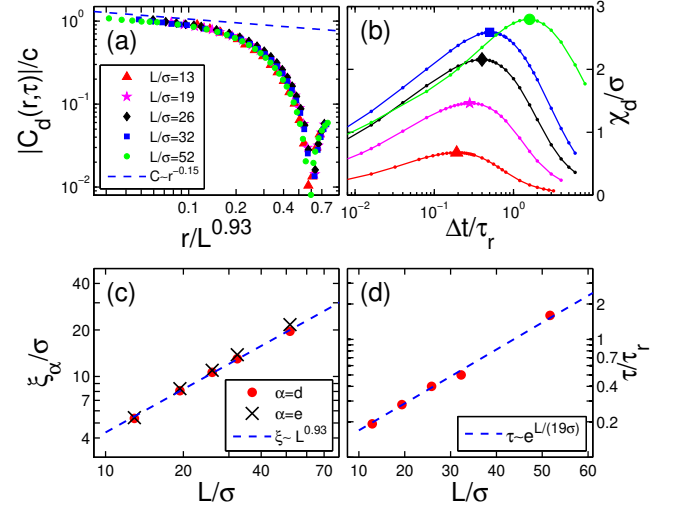


FIG. 3: (color online) (a) Modulus of the spatial displacement correlation function  $C_d(r, \Delta t = \tau)$  as a function of  $r/L^{0.93}$  for  $\phi = 0.6$  and  $Pe = 272$ . We show  $C_d$  at the time  $\tau$  of maximal cooperativity.  $C_d$  is scaled by  $c = 0.47, 0.55, 0.55, 0.54, 0.37$  for  $L/\sigma = 13, 19, 26, 32, 52$ , respectively. (b) Cooperativities  $\chi_d(\Delta t)$  of the various system sizes  $L$  (symbols indicate  $\tau$ ). (c) Correlation lengths of the displacements  $\xi_d(\tau)$  and the orientations  $\xi_e$  as a function of system size  $L$ . (d) Exponential growth of the build-up time  $\tau$  with  $L$ .

tions, which originate from small regions of polar order at the gas-fluid interface, are very weak and  $\chi_e$  is an order of magnitude smaller than  $\chi_d(\tau)$ .

Motivated by snapshots (Fig. 2) and movies [24], we propose the following mechanism behind the observed collective dynamics. Consider first a smooth (flat) interface between the gas and fluid phase: fast moving gas-phase particles bump into the interface and remain there until rotational diffusion leads to an approximately parallel orientation of  $\mathbf{e}$  to the interface [29]. In concave regions of a curved interface, however, the reorientation of  $\mathbf{e}$  requires more time until escape is possible, i.e., particles are effectively trapped. By contrast, particles in convex regions (protrusions) slide easily into a neighboring concave regions. This self-amplifying process accumulates particles with distinct polar order in concave regions and thereby triggers streams of orientationally disordered particles deep inside the fluid phase. Due to mass conservation the particles stream into a neighboring gas droplet or toward the droplet which itself activated the flow. As a result, further deformations of droplets are produced and hence new instabilities are induced.

Variation of the activity, characterized by  $Pe$ , substantially affects the structure and dynamics of the suspension. We illustrate this behavior for  $\phi = 0.6 > \phi_G$ . Below a critical Péclet number  $Pe_c(\phi) \approx 120$ , the system does not phase separate, but remains homogeneous and any sign of local polar order, which is related to the presence of a fluid-gas interface, disappears below  $Pe_c$ , i.e.,

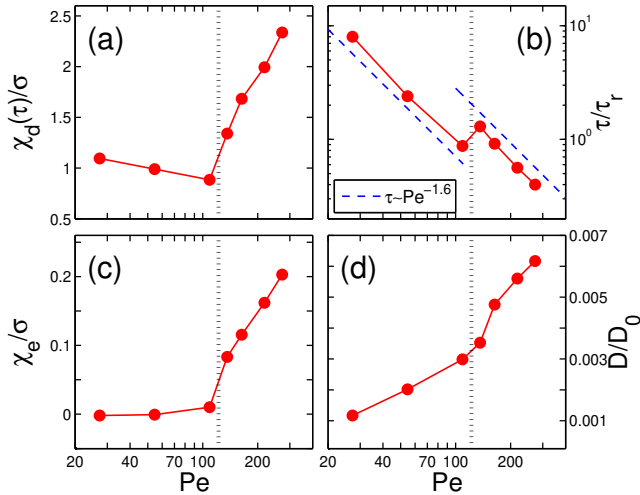


FIG. 4: (color online) (a) Cooperativity  $\chi_d(\tau)$ , (b) build-up time  $\tau$ , (c) global polar correlation  $\chi_e$  and (d) long-time diffusion constant  $D$  (normalized by  $D_0 = D_t + V_0^2/(6D_r)$ ) as a function of  $Pe$  for the packing fraction  $\phi = 0.6$  and the system size  $L/\sigma = 28$ . Dashed line indicates  $Pe_c \approx 120$ .

$\chi_e \approx 0$ , see Fig. 4(c). Thereby, the dynamical behavior of the systems change drastically across  $Pe_c$ . As seen in Fig. 4(a), the cooperativity  $\chi_d$  decreases strongly while approaching  $Pe_c$  from above and is nearly constant below  $Pe_c$ . The maximal cooperativity builds up at later times  $\tau$  with decreasing  $Pe$ , see Fig. 4(b). As a result, collective motion below  $Pe_c$  appears on diffusive time scales,  $\tau > \tau_r$ , and becomes increasingly reminiscent of an inactive supercooled fluid [25]. Finally, the particle dynamics is drastically slowed down at small  $Pe \approx 10$ , where the system starts to freeze, as indicated in the phase diagram in Fig. 5. In Fig. 4(d) we show the diffusivity  $D$  normalized by the corresponding value of a free self-propelled particle,  $D_0 = D_t + V_0^2/(6D_r)$ . Although we are above  $\phi_G$ ,  $D/D_0$  is finite and is an increasing function of  $Pe$ . The latter suggests a shift of the glass transition to larger  $\phi$  with increasing activity [30, 31].

We collect all our results in a phase diagram spanned by  $Pe$  and  $\phi$ , see Fig. 5. For high  $Pe$ , the homogeneous phase is unstable over a broad range of packing fractions  $\phi$ , as explained above. The unstable range decreases with decreasing  $Pe$  (the lower bound is predicted to obey  $\phi_c \sim Pe^{-1}$  [12]). Below  $Pe \approx 30$  phase separation disappears for all  $\phi$ . Except for large  $\phi$  and low  $Pe$ , where crystalline domains are formed, the dynamics is fluid-like. We expect jamming to occur for  $\phi \rightarrow \phi_{RCP}$  in the limit of very large  $Pe$ .

The phase separation as a function of  $\phi$  and  $Pe$  can be understood as follows. The pressure  $p_{HS}(\phi)$  of a hard sphere fluid increases with  $\phi$  and diverges at RCP for the metastable branch [21]. Self-propelled particles at low  $\phi$  easily overcome this pressure, coagulate due to their

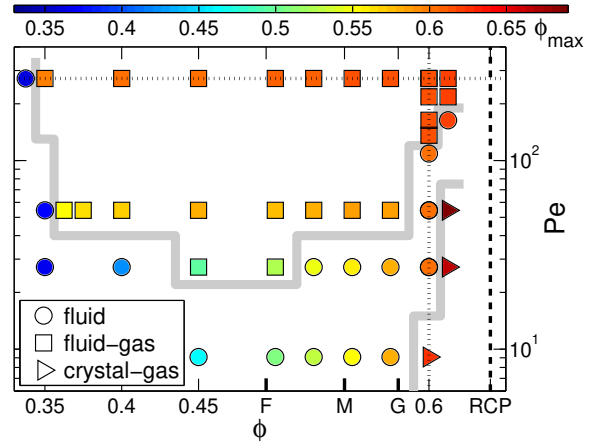


FIG. 5: (color online) Phase diagram of the active suspension spanned by  $Pe$  and  $\phi$ . Indicated by symbols are the homogenous fluid phase ( $\circ$ ), the fluid-gas phase ( $\square$ ) and the crystal-gas (or pure crystal) phase ( $\triangleright$ ). The equilibrium transition points of hard spheres, namely, freezing ( $\phi_F = 0.494$ ), melting ( $\phi_M = 0.545$ ), glass-transition point ( $\phi_G \approx 0.58$ ), and random close packing ( $\phi_{RCP} \approx 0.64$ ), are marked by F, M, G, RCP, respectively. The most probable  $\phi_{local}$  is color-coded, i.e., in the two-phase region one can read off the density of the dense phase.

slow-down during collisions (overdamped dynamics) and hence form clusters; such a behavior can be interpreted as an *effective* attractive interaction [32]. The density within the cluster  $\phi_f$  adjusts such that  $p_{HS}(\phi_f)$  balances the active pressure. An initially homogenous system can only phase separate if the active pressure exceeds  $p_{HS}(\phi)$ .

Suspension of active particles without an alignment rule exhibit on broad range of fascinating structural and collective dynamical effects. Not all of them have been addressed in this letter. In particular, the crossover from the equilibrium phase behavior to the regime at low  $Pe$  deserves further attention. In that respect, recent studies indicate a shift of the liquid-crystal coexistence in 2D [13] and of the glass transition in 3D [30, 31] to higher  $\phi$  with increasing activity in consistence with our findings. Studies of active fluids at low  $Pe$  may shed light on the dynamics in glassy systems in a complementary way to external fields like shear.

The authors would like to thank M. Abkenar, T. Auth, J. Horbach, S. Poblete, G. M. Schütz and M. Sperl for helpful discussions. Financial support by the VW Foundation (VolkswagenStiftung) within the program *Computer Simulation of Molecular and Cellular Bio-Systems as well as Complex Soft Matter* is gratefully acknowledged.

\* Electronic address: a.wysocki@fz-juelich.de

† Electronic address: r.winkler@fz-juelich.de



<sup>‡</sup> Electronic address: g.gompper@fz-juelich.de

- [1] T. Vicsek and A. Zafeiris, *Phys. Rep.* **517**, 71 (2012).
- [2] T. E. Angelini, E. Hannezo, X. Trepát, M. Marquez, J. J. Fredberg, and D. A. Weitz, *Proc. Natl. Acad. Sci. USA* **108**, 4714 (2011).
- [3] I. H. Riedel, K. Kruse, and J. Howard, *Science* **309**, 300 (2005).
- [4] D. Kearns, *Nat. Rev. Microbiol.* **8**, 634 (2010).
- [5] H. H. Wensink, J. Dunkel, S. Heidenreich, K. Drescher, R. E. Goldstein, H. Löwen, and J. M. Yeomans, *Proc. Natl. Acad. Sci. USA* **109**, 14308 (2012).
- [6] F. Peruani, A. Deutsch, and M. Bär, *Phys. Rev. E* **74**, 030904 (2006).
- [7] Y. Yang, V. Marceau, and G. Gompper, *Phys. Rev. E* **82**, 031904 (2010).
- [8] E. Lauga and T. R. Powers, *Rep. Prog. Phys.* **72**, 096601 (2009).
- [9] Y. Fily and M. C. Marchetti, *Phys. Rev. Lett.* **108**, 235702 (2012).
- [10] I. Theurkauff, C. Cottin-Bizonne, J. Palacci, C. Ybert, and L. Bocquet, *Phys. Rev. Lett.* **108**, 268303 (2012).
- [11] J. Palacci, S. Sacanna, A. P. Steinberg, D. J. Pine, and P. M. Chaikin, *Science* **339**, 936 (2013).
- [12] G. S. Redner, M. F. Hagan, and A. Baskaran, *Phys. Rev. Lett.* **110**, 055701 (2013).
- [13] J. Bialké, T. Speck, and H. Löwen, *Phys. Rev. Lett.* **108**, 168301 (2012).
- [14] We employ a steep (shifted) Yukawa potential  $V(r) = 5k_B T \exp[-\kappa(r - \sigma)]/[\kappa(r - \sigma)]$  for  $r > \sigma$  with  $\kappa\sigma = 60$ .
- [15] J. R. Howse, R. A. L. Jones, A. J. Ryan, T. Gough, R. Vafabakhsh, and R. Golestanian, *Phys. Rev. Lett.* **99**, 048102 (2007).
- [16] H.-R. Jiang, N. Yoshinaga, and M. Sano, *Phys. Rev. Lett.* **105**, 268302 (2010).
- [17] G. Volpe, I. Buttinoni, D. Vogt, H.-J. Kummerer, and C. Bechinger, *Soft Matter* **7**, 8810 (2011).
- [18] K. Drescher, K. C. Leptos, I. Tuval, T. Ishikawa, T. J. Pedley, and R. E. Goldstein, *Phys. Rev. Lett.* **102**, 168101 (2009).
- [19] C. H. Rycroft, *Chaos* **19**, 041111 (2009).
- [20] P. N. Pusey and W. van Meegen, *Nature* **320**, 340 (1986).
- [21] R. D. Kamien and A. J. Liu, *Phys. Rev. Lett.* **99**, 155501 (2007).
- [22] K. Michielsen and H. D. Raedt, *Phys. Rep.* **347**, 461 (2001).
- [23] K. E. Davis, W. B. Russel, and W. J. Glantschnig, *Science* **245**, 507 (1989).
- [24] See Supplemental Material at <http://link.aps.org/supplemental/xxx> for videos.
- [25] B. Doliwa and A. Heuer, *Phys. Rev. E* **61**, 6898 (2000).
- [26] A. Cavagna, A. Cimarelli, I. Giardina, G. Parisi, R. Santagati, F. Stefanini, and M. Viale, *Proc. Natl. Acad. Sci. USA* **107**, 11865 (2010).
- [27] X. Chen, X. Dong, A. Be'er, H. L. Swinney, and H. P. Zhang, *Phys. Rev. Lett.* **108**, 148101 (2012).
- [28] H. Tanaka, T. Kawasaki, H. Shintani, and K. Watanabe, *Nat. Mater.* **9**, 324 (2010).
- [29] J. Elgeti and G. Gompper, *Europhys. Lett.* **101**, 48003 (2013).
- [30] W. T. Kranz, M. Sperl, and A. Zippelius, *Phys. Rev. Lett.* **104**, 225701 (2010).
- [31] L. Berthier and J. Kurchan, *Nat. Phys.* **9**, 310 (2013).
- [32] J. Tailleur and M. E. Cates, *Phys. Rev. Lett.* **100**, 218103 (2008).